Heat, Salt, and Surface Elevation Changes in the Global Ocean and Their Uncertainties

Part 4 of: A Twenty-Year Dynamical Oceanic Climatology: 1994-2013

Carl Wunsch*

Department of Earth and Planetary Sciences

Harvard University

Cambridge MA 02138

email: cwunsch@fas.harvard.edu

October 20, 2017

Abstract

Estimates are made of the 20-year time means and their time evolution over that period of oceanic temperature, salinity, and sea surface height, during the data-dense interval 1994-2013—along with heuristic estimates of their uncertainties. Values are computed from a state estimate calculated from a free-running ocean-ice general circulation model whose initial/boundary conditions and internal mixing coefficients have been adjusted to produce consistency with nearly all globally available measurements. The essential step of separating stochastic from systematic or deterministic elements of the fields is explored by suppressing the globally correlated components of the fields. Uncertainties reflecting the stochastic elements of the state estimate are then calculated from bootstrap and jackknife estimates. Trends are estimated as 2.1 ± 0.1mm/y in elevation, $0.00107\pm3.6\times10^{-5\,\circ}$C/y, and $-3.2\times10^{-5}\pm1.5\times10^{-6}$g/kg/y for surface elevation, temperature and salt, with uncertainties representing only the estimated stochastic component of error. The temperature change correspnds to a 20-year average ocean heating rate of 0.48 ± 0.002 W/m^2 of which 0.1W/m^2 arises from the geothermal forcing.

1 Introduction

Many papers have been directed at estimating, directly from observations, multi-decadal ocean heat uptake (Purkey and Johnson, 2010; Lyman et al., 2014), salinity change as an indicator of

---

*Also, Dept. of Earth, Atmospheric and Planetary Sciences, MIT

₂₄ fresh-water injection (Wadhams and Munk, 2004; Boyer et al., 2005), and sea level (elevation)

₂₅ changes (Nerem et al., 2006; Cazenave et al., 2013) or all together (Levitus et al., 2003; Peltier et

₂₆ al., 2009; Forget and Ponte, 2015). Many more such calculations have been published than can be

₂₇ listed here. A great difficulty with most of these estimates is the historical inhomogeneity in the

₂₈ various data sets employed, and the consequent use of nearly untestable statistical hypotheses

₂₉ used to extrapolate and interpolate into data sparse times and places (see Boyer et al., 2016 and

₃₀ Wunsch, 2016 for generic discussions). A number of papers have proclaimed "closure" of the sea

₃₁ level change budget, but that is accomplished through large and uncertain error budgets of the

₃₂ various components.

₃₃ Ocean general circulation models (GCMs) and coupled climate models have also been used to

₃₄ calculate space- and time-mean oceanic temperature (T), salinity (S) , and sea surface elevations

₃₅ (η). Most models, including the ECCO system (Estimating the Circulation and Climate of

₃₆ the Ocean; Wunsch and Heimbach, 2013; Forget et al., 2015), compute the ocean state in a

₃₇ deterministic fashion. That is, given initial conditions and time-varying meteorological boundary

₃₈ conditions, the model time-steps the state vector, $\mathbf{x}(t)$, as though the external fields, including

₃₉ initial conditions, were fully known. Ensemble (Monte Carlo) methods attempt to estimate the

₄₀ uncertainties of the state at a particular time, usually a forecast time, by computing families of

₄₁ disturbed initial and/or boundary conditions.

₄₂ A general discussion of the accuracy or precision of climate models does not appear to exist.

₄₃ As in all systems, errors will always include systematic ones e.g., from lack of adequate resolution

₄₄ or improperly represented air-sea transfer processes, amongst many others. Stochastic errors

₄₅ will arise from noisy initial and boundary conditions of all types, as well as rounding errors, and

₄₆ interior instabilities of many types, both numerical and physical. Analysis of systematic and

₄₇ stochastic errors requires completely different methods.

₄₈ The purpose of this paper is two-fold: to produce best estimates of oceanic T, S, η values

₄₉ and their variability from the nearly homogeneous (in the observational network sense) data

₅₀ sets 1994-2013, and to make a start towards the essential separation of random from systematic

₅₁ or deterministic processes. Estimation of systematic errors requires totally different procedures,

₅₂ involving a near line-by-line discussion of the individual computer codes used to calculate oceanic

₅₃ states. Both error types will be different in calculations of the mean state and in their temporal

₅₄ and spatial changes.

₅₅ For "state estimation" as done in ECCO (see Forget et al., 2015; ECCO Consortium 2017a,b;

₅₆ Fukumori et al., 2017), two major obstacles loom if Monte Carlo methods are to be used: (1)

₅₇ the immense state and control vector dimensions; (2) The absence of quantitative estimates

₅₈ (probability distributions) of the stochastic contributions in the initial/boundary conditions

and effectively stochastic structures generated by internal instability and turbulence. The same obstacles to uncertainty calculation loom in *any* ocean or coupled-climate model run for long times whether or not based upon combinations with data.

A number of methods exist for calculating uncertainties in systems such as that of ECCO. To the extent that the system is linearizable, the method-of-Lagrange-multipliers/adjoint used there can be shown (e.g., Wunsch, 2006) to have identical uncertainties to those obtained from sequential estimates, such as the Rauch-Tung-Striebel (RTS) smoother.[1] This approach is very well understood and is practical for small systems (Goodwin and Sin, 1981; Brogan, 1991; Wunsch, 2006). It involves calculated covariance matrices that are square of the state vector dimension and of the control vector dimension at any time, t. For the ECCO version 4, state vector dimension at each time step is approximately 39 million, a number far too large for the covariances to be calculated or manipulated, much less understood. With a time-step of one hour over 25 years, the total evolving ECCO state vector, if stored, would be about 30 terabytes, without including the covariance matrices. Similar dimensions and issues apply to the system control vector.

Other methods include calculation of inverse Hessians (Kalmikov and Heimbach, 2014), sometimes using Lanczos methods. Hypothetically, one could solve a Fokker-Planck equation corresponding to the model (Gardiner, 2004) and its initial/boundary condition, or the prediction-particle filtering methods of Majda and Harlim (2012). None of these methods is computationally practical for the global ocean or climate system with today's computers—although that should gradually change in the future.

Nonetheless, some form of useful uncertainty estimate is necessary for values calculated from models, whether from ordinary forward calculations, or from a state estimate. So for example, as described by ECCO Consortium (2017a), Fukumori et al. (2017), the 20-year average ocean temperature is 3.5319°C found from the $N = 2.4 \times 10^6$ volume weighted grid points of the model (centers of cells). How reliable is that number? On the one hand, it is extremely accurate up to the machine precision of 2^{-64}. A standard error might be calculated by dividing the variance of the volume-weighted elements by 2.4×10^6, but such a number is meaningless: (1) much of the thermal structure of the ocean is deterministic on the large-scale—and with other effectively permanent sub-basin scale structures—stable over 20+ years. Treating that structure as stochastic would be a major distortion. (2) The distribution of values is very inhomogeneous

---

[1] The RTS smoother employs the Kalman filter as a sub-component in the numerical algorithm. Kalman filters are predictors and should not be confused with general smoothing estimators. In any case, true Kalman filters, which require continual updating of the covariance matrices, are *never* used with realistic large-scale fluid problems—the dimensionality is overwhelming. In practice, the prediction numerics are usually approximated forms of *Wiener filters*, employing temporally fixed, guessed, covariances.

over the three-dimensional volume and any supposition of uniform probability densities or of near-Gaussian values is incorrect (see Fig. 1). An empirical probability density could be fit to the model output, but as noted, that would lead to incorrect results as much of this structure is contained in the deterministic elements.

Parts of the ocean structure and of the meteorological forcing fields are best regarded as deterministic processes over decades. For example, the depth and properties of the main thermocline, or of the dominant wind systems, do not vary significantly over 20 years. Superimposed upon the initial and boundary conditions are noise fields best regarded, in contrast, as stochastic.

When integrated through a time-stepping fluid model, the stochastic elements, even disturbances that are white noise in space and/or time, will give rise to complex structured fields (see for example Fig. B5 of Wunsch, 2002). A crux of the uncertainty problem for model outputs then is to separate the deterministic from the stochastic elements. Ensemble methods, generated by stochastic perturbations of initial/boundary conditions/parameters, face the same difficulty: What are the appropriate joint probability distributions to use in generating the ensembles (e.g. Evensen 2009)?[2] To the extent that the stochastic influence can be regarded as perturbations about a stable deterministic evolution, the probability densities will be centered about deterministic fields, as in Eq. (3.5.9) of Gardiner (2004). Systematic errors will remain as part of the deterministic components, and must be dealt with separately.

What follows is largely heuristic: methods for separation of deterministic from stochastic elements in large volumes of numbers do not appear to have been widely explored. (This issue should not be confused with the problem of separating "deterministic chaos" from true stochastic elements familiar in dynamical systems theory; e.g. Strogatz, 2015).

2   Mean Values

A start is made with time-mean three-dimensional fields which permits introducing the basic ideas while greatly reducing the volume of numbers required. A supposition is thus made that *only the time average fields are available* and sampled, temporarily suppressing the information contained in the time-variability. Suppression of the deterministic component, so as to leave a stochastic field, is required for both mean and time variations.

Temperature

Consider the problem of determining the 20-year global ocean average temperature and its corresponding uncertainty. A 20-year average, computed 50 years in the future, might usefully

---

[2]Computationally practical ensemble dimensions remain orders of magnitude smaller than any reasonable estimate of the number of degrees-of-freedom.

be compared with the present 20-year average. The immediate simplification made is to assume that only the 20-year average model output is available, not the underlying time variation. Hourly values of the state estimate, averaged over 20-years, 1994-2013, produce point-wise calculated mean potential temperatures, $\bar{T}_i$. Mean temperature at one depth can be seen in Fig. 2, displaying the classical large-scale features that are clearly deterministic over 20-years with superimposed stochastic elements. When the three-dimensional field is weighted by the relative volume contribution, a_i, from the spatially varying model grid, a_i, $(\sum a_i = 1)$ produces a population $\theta_i = \bar{T}_i a_i$ drawn from an unknown probability distribution, a probability distribution centered about the (also unknown) deterministic structures. As stated above, the raw mean value of the 20-year averages at all grid values is,

$$\tilde{m} = \sum_{1}^{N} a_i \bar{T}_i = 3.5319^{\circ}C,$$

with unknown reliability.

The basic notion here is to use the bootstrap and related jackknife methods in the elementary sense described by Efron and Tibsharani (1993), Mudelsee (2014), and others. That is, we begin by generating 50 bootstrap samples of N values (resampling with replacement from the N values, θ_i). The result is shown in Fig. 3 with a bootstrap mean of $3.5318^{\circ} \pm 0.0024^{\circ}$ almost identical to the ordinary average.[3] These values are, however, incorrect: *the basic assumption of the bootstrap is that the values making up the subsampled population are independent, identically distributed (iid), values.* Any assumptions that stochastic elements in cold, deep, temperatures are drawn from the same population as the much warmer near-surface values, or that this structure is dominantly stochastic, cannot be correct.

An ad hoc assumption will now be made that the *strongest globally spatially varying structures represent the deterministic component.* This assumption is based on considerations of physics—that any three-dimensional, globally correlated structure can only have been generated by very long-term effectively systematic processes—and not upon any statistical methodology. If a process can be rendered indistinguishable from white noise, then at zero-order most covariance structure has been removed.[4] Stochastic integration does produce correlated structures (e.g., Fig. B5 in Wunsch, 2002), but 20 years is sufficiently brief that assumptions of mainly local covariance of the stochastic elements, and that globally correlated fields are effectively deterministic on multi-decadal time-scales, are not unreasonable. A plausible, if not demonstrable,

---

[3]Worthington (1981) estimated the global average potential temperature as 3.51°C, using a much more restricted data set, and provided no uncertainty estimate. His value is remarkably close to the present one but was meant to apply to the total historical period ending about 1977. See the discussion in Wunsch (2016).

[4]An alternative, not used here, would be a spectral expansion in spherical harmonics and a choice of vertical basis functions, and the exploitation of the non-random character of the coefficients of the deterministic elements.

assumption can be made that the residual values, $\theta_i' = \left(a_i \bar{T}_i\right)'$, drawn anywhere from each of the 50-levels of the model are iid if the overall spatial covariance has first been removed and that variances are nearly uniform.

The 3-dimensional matrix of volume-weighted temperatures is, $\boldsymbol{\Xi}\left(\lambda_i, \phi_j, z_k\right)$, written with columns in longitude, latitude, and depths. Map this three-dimensional matrix into two dimensions by stacking the latitude columns, $\boldsymbol{\Xi}'\left(r_p, z_k\right)$ where r_p is just a reordering of longitude and latitude. Write $\boldsymbol{\Xi}'$ as its singular value decomposition,

$$\boldsymbol{\Xi}'\left(r_p, z_k\right) = \mathbf{U}_K \boldsymbol{\Lambda}_K \mathbf{V}_K^T, \ \ K \le 50, \tag{1}$$

where the vertical dimension is described by the 50 vectors making up the columns of matrix $\mathbf{V}$. K is the number of non-zero singular values and hence is the rank of $\boldsymbol{\Xi}'$. ($\mathbf{U}_K, \mathbf{V}_K$ contain the first K columns, etc. and $\boldsymbol{\Lambda}_K$ is a $K \times K$ diagonal matrix.) The fractional value of the squared singular values, $\lambda_i = diag(\boldsymbol{\Lambda}_K)_i$, as the sum,

$$S(J) = \frac{\sum_{j=1}^{J} \lambda_j^2}{\sum_{j=1}^{50} \lambda_j^2}, \ \ J = 1, ..., K \tag{2}$$

is shown in Fig. 3 and representing the cumulative variance by singular vector pair. The first singular vector pair $\mathbf{u}_1, \mathbf{v}_1$ accounts for over 90% of the variance (compare Fukumori et al., 1991) and including the second pair, $\mathbf{u}_2, \mathbf{v}_2$ raises it to about 96%. Fig. 4 shows the reduction in the range with depth of the spatial variance of temperature by removal of the first two singular vector pairs. In an ideal situation, the variance of an iid would be uniform with depth.

Subtracting the lowest three pairs produces,

$$\boldsymbol{\Xi}_1'\left(r_p, z_k\right) = \boldsymbol{\Xi}' - \lambda_1 \mathbf{u}_1 \mathbf{v}_1^T - \lambda_2 \mathbf{u}_2 \mathbf{v}_2^T - \lambda_3 \mathbf{u}_3 \mathbf{v}_3^T = \sum_{\mathbf{j=4}}^{\mathbf{50}} \lambda_j \mathbf{u}_j \mathbf{v}_j^T, \tag{3}$$ {projection1}

the projection on the highest 47 singular vectors, and which reduces the 2-norm of $\boldsymbol{\Xi}'$ by 96%. The horizontal spatial patterns of the first three pairs, at 105m, are shown in Fig. 5. $\mathbf{u}_1$ carries the major climatological fields, with a zonal banding of low absolute values at high latitudes, with mid-latitude maxima, and a more extreme Atlantic than Pacific. In the vertical (Fig. 5d), $\mathbf{v}_1$ generally decays with depth, albeit with vertically localized mild maxima. $\mathbf{u}_2$ and $\mathbf{v}_2$ convey a tropical structure, rapidly diminishing with depth. Somewhat arbitrarily, the first three pairs are here deemed to carry the deterministic structure, and the residual (Fig. 6) is assumed to represent the stochastic field. This projection onto the least correlated components leaves some obvious spatial covariances both in the vertical and the horizontal—as would result from integrated stochastic fields—and this residual is assumed to be stochastic. Although it

6

177 appears not possible to test these assumptions directly at the present time, they do provide a
178 way forward.

179   When the bootstrap is applied to the residual field, the temperature standard deviation is
180 reduced to $6.9 \times 10^{-4}°$C and which is tentatively accepted as the best estimate of the standard
181 error uncertainty owing to the stochastic elements. The distribution of values (Fig. 1) has
182 become unimodal and symmetric without the pronounced skewness of the original distribution.

183   Much structure exists with latitude, longitude, and depth both in the suppressed singular
184 vectors and in the residuals, here and in the fields described below. Understanding of the details
185 of these structures takes one deep into the physics of temperature and salinity in the ocean and
186 ultimately each will necessitate a separate discussion of their distributions and changes.

187   *Salinity*

188   The time mean salinity, (34.7281 g/kg), determined from the volume-weighted values $a_i \overline{S_i}$ has
189 the histograms shown in Fig. 7.[5] The singular vectors and bootstrap histories are shown in Fig.
190 8. If the first-3 SVD pairs of $a_i \overline{S_i}$, (Fig. 9) containing about 96% of the variance, are subtracted
191 (Fig. 10), the standard error is ± 0.010g/kg. For reference, using $\Delta h = -h_0 \Delta S/S_0$ where h_0, S_0
192 are the starting values of mean depth and salinity (Munk, 2003), the uncertainty ± 0.010g/kg
193 corresponds to a freshwater change uncertainty of about ± 1.1m . This value may seem surpris-
194 ingly large, but it simply says that the salinity data permit inference of the total amount of
195 added freshwater of about $\Delta h = 1.1$m out of a total average depth of about $h = 3800$m, or about
196 0.03%, which by most standards is remarkable accuracy. One can hope that a comparison 50
197 years hence will *not* find changes Δh which are significantly different from zero!

2.1   Sea Surface Height/Dynamic Topography

199 Mean sea surface height, η, the "dynamic topography" in the present ocean state, can in principle
200 be compared to its value determined as a 20-year average, 50 years or any other time interval into
201 the future. Values in the ECCOv4 state estimate are determined relative to the best available
202 geoid known today (the GRACE-determined values). The dynamical variables are the horizontal
203 gradient elements and thus if in the future a different geoid is used, offset by a constant from the
204 one used in ECCO, that change would be of no significance. On the other hand, care would be
205 needed in the future to accommodate changed geoids with for example, higher spatial resolution.

206   The assumption used so far, that globally covarying fields can be interpreted as the determin-
207 istic components, is physically sensible for temperature and salinity. For η however, the ability

---

[5]Worthington's (1981) value was 34.72g/kg, again with no stated uncertainty, but very close to the present
value, although pertaining to the historical period prior to about 1977.

of the ocean to transmit barotropic signals globally within a few days, makes the assumption dubious. Nonetheless, with this caveat, the global time-mean value of η and an estimate of its accuracy is calculated within the model context. The spatial mean of the field in Fig. 11 is 0.048 in the interval 1994-2013.

In contrast to the temperature and salinity fields, time-mean η exists only in two dimensions. Thus the singular vectors are calculated treating longitude and latitude as separate defining fields (the matrix has a latitude-longitude structure). Removal of the first 3 singular vector pairs results in Fig. 12. Applying the bootstrap to this field produces a mean standard error of 6.7×10^{-4}m. Thus the final estimate of the time mean η is 4.8 ± 0.1 cm and which hypothetically could be compared to a time-mean relative to the geoid computed decades hence.

3   Time Changes: Difference of Last and First Years

In dealing with time changes, of intense interest for climate understanding, the difference between two yearly-averages, years t_1, t_2, should largely remove the deterministic components contained in the initial/boundary conditions. A trend, e.g. in exchange of heat between ocean and atmosphere as a part of the global warming signal and part of the surface boundary conditions, might be regarded as deterministic. But, as has been noted in numerous publications (e.g., Ocaña et al., 2016), with a 20-year record, the duration is far too short to distinguish a true deterministic trend from the long-term stochastic shifts characteristic of red-noise processes, and here any trend present is treated as though arising from a stochastic process. Discussion here of temporal changes is done in two ways: (1) the value of the differences of the first and last years 20-years apart, and which makes no inferences about the nature of the trend. (2) The bootstrapped or jackknifed estimate of the trends, assumed to be linear ones.

3.1   Temperature/Heat Content

One interesting example is the comparison of the mean ocean temperature in 1994 to what it was in 2013 (shown for two depths in Figs. 13)—as a constraint on the rates of global warming. This difference is a static field and can be analyzed in the same fashion as the time-mean was treated. The spatial pattern of warming and cooling is a complicated one with large-scale structures corresponding to known physical regimes, e.g., the eastern tropical Pacific, the near-Gulf Stream system/subpolar gyre, the Southern Ocean. Note that the two estimates are *not* independent ones—they are connected through the time-evolving equations of motion.

To the extent that any systematic error in the ECCO system is time-independent, it will be subtractive in the time-difference. Without drawing any concrete inference about the validity of

8

that statement, Fig. 14 shows the first few SVD pairs and the variance reduction with depth can be seen in Fig. 15 and the histogram of difference values of $a_i\left(T_i\left(t_2\right) - T_i\left(t_1\right)\right)$ is shown in Fig. 16. The latter is much closer to a Gaussian than either of the two annual means alone (Fig. 1). The mean difference in temperature is found to be $0.0204°C$. Assuming that the full difference can be treated as a stochastic field, the bootstrap standard deviation is $1.0 \times 10^{-4}°C$. Removing the first two singular vector pairs decreases the standard deviation to $7.0 \times 10^{-5}°C$ and thus the difference value appears highly significant in either case, and is thus $0.0204 \pm 0.0001°C$.

With a fixed heat capacity of $c_p = 3994\text{J}/°C/\text{kg}$ and an ocean mass of 1.37×10^{21} kg, the change in heat content is about $1.1 \times 10^{23} \pm 5.5 \times 10^{20}$ J. This value corresponds to a net heat uptake of 0.48 ± 0.002 W/m^2, again including 0.095W/m^2 from the geothermal input (ECCO2017a). This accuracy is encouraging, but returns attention to the possible systematic errors in the model and data that could affect the rate of enthalpy gain. The geothermal heating rate is also partially uncertain.

3.2 Salinity/Freshwater

The pattern of differences of salinity between 1994 and 2013 (Fig. 17) and is already visually somewhat stochastic in character. Histograms, the bootstrap history, and the singular vectors are shown in Fig. 18.

The mean salinity change between the two years is $(-5.5\pm0.10)\times10^{-4}$ g/kg from the bootstrap estimate with two singular vector pairs removed. A salinity change of -5.5×10^{-4} corresponds to a freshwater addition of 5 ± 0.1cm over 20 years, or 2.5 ± 0.5mm/y.

3.3 Surface Height

The difference in height over 20 years (Fig. 19) is 4.01 ± 0.018 cm, or an average change of 2.005 ± 0.01mm/y where the standard error is obtained from the bootstrap with three singular vector pairs removed. (Nerem et al., 2006, quote a rate from altimeter data alone, as 3.1 ± 0.4mm/y. Although the estimates are not independent—the state estimate uses all the altimeter data—in a formal sense, no conflict exists between the values.) The total is all accounted for, within one standard error, by the salinity change. That leaves perhaps 0.5mm/y, within two standard errors, for the thermal contribution. The thermal contribution is complex because the coefficient of expansion of sea water is a complicated function of the ambient T, S, and pressure, P, fields. The η fields estimated here are derived from the changing density field, including all of T, S, P. But accurately, additively separating the contributions of changing T, S, and in particular given the large equivalent fresh water uncertainty, is not possible here.

9

4 Estimated Linear Trends

4.1 Temperature/Heat Content

The integrated temperature to various depths is shown in Fig. 20. The best fitting, assumed linear, trend over 20 years is sought. Whether deterministic or a red-noise random walk is immaterial at this stage. The mean slope for the top-to-bottom change is $0.0011 \pm 3.6 \times 10^{-5\circ}$C/y. Standard error is computed from a bootstrap of the full field (Fig. 21), under the assumption that the time differences are basically stochastic and which likely slightly overestimates the uncertainty. (A jackknife estimate was identical.) The mean slope implies a change over 20 years of $0.02 \pm 7.2 \times 10^{-4\circ}$C and which necessarily, because of the noise, differs slightly from the value computed between first and last years. The temporal coefficients $\mathbf{v}_i$ of the annual spatial means are displayed in Fig. 22 and showing the noisy trend in the lowest pattern $\mathbf{u}_1$.

Although the temperature change as a function of depth is shown in Fig. 20, only the top-to-bottom integrals are used here. Integrals taken to intermediate depths, or intermediate densities, are related to the potential and internal energies of an open-system, and thus are not interpretable in terms of net external inputs. Depth dependence does provide insights into the physics governing heat redistribution (see e.g., Liang et al., 2017), but that subject is not pursued here.

4.2 Salinity Trends

Integrated salt anomalies are displayed for each year to several depths in Fig. 23. An overall freshening, top-to-bottom is evident, including a slight increase in salinity at and below 3600m. This abyssal change accompanies the general cooling seen below 3600m in Fig. 20, but this physics is not further described here.

Fig. 24 shows the lowest SVD pairs. The mean bootsrapped salinity trend over the 20 years is $-3.2 \times 10^{-5} \pm 1.52 \times 10^{-6}$g/kg y for a net salinity change from the trend of $6.4 \times 10^{-4} \pm 0.304 \times 10^{-4}$g/kg. (For comparison, Boyer et al., 2004, estimated the trend as 5.4×10^{-4}g/kg/y from a much longer and much more inhomogeneous data set. No uncertainty was specified.) The corresponding freshwater change from the present estimate is a net 7.0 ± 0.3cm addition over 20 years.

4.3 η Trends

Fig. 25 displays the annual spatial average values of η and the first differences between sequential years. The spatial patterns do not show a single dominant singular value (10 of them are required

to account for 90% of the variance). Fig.26 displays $\mathbf{u}_1$ and its temporal coefficient, and clearly accounts for the trend-like behavior seen overall.

An estimate of the trend is $2.1 \times 10^{-3} \pm 7.4 \times 10^{-5}$m/y, again from a bootstrap of the full annual spatial average, about 2mm/y. The corresponding mean surface height change is then 4.1±0.15cm over the 20 years.

5 Discussion

The best fitting linear elevation trend is 2.1±0.1mm/y. Twenty-year average global temperature and salinity linear trends are $0.00107 \pm 3.6 \times 10^{-5}$°C/y and $-3.2 \times 10^{-5} \pm 1.52 \times 10^{-6}$g/kg/y respectively. Net changes, based upon the spatial mean differences of 2013 and 1994 are 4.0 ± 0.01cm, $0.0204 \pm 1.0 \times 10^{-4}$°C, $-5.46 \pm 1.0 \times 10^{-5}$g/kg. Listed uncertainties are approximate one-standard deviations derived from the stochastic elements. In general, histograms of the inferred residual stochastic fields become unimodal without long tails, apart from isolated outliers.

Although 20-year time-means and changes in the global average oceanic heat, salt, and dynamic topography (sea surface height) have been estimated here, the important by-product is the provision of useful uncertainties from the random error in the values when computed from general circulation or climate models. Results are almost entirely heuristic, but the approach using resampling (bootstrap and jackknife) methods can perhaps be made rigorous. In particular, methods for separating deterministic and stochastic elements of the three-dimensional, time-dependent fields, in the absence of real knowledge of the probability distributions, should be explored. Apparent stochastic two-standard deviation uncertainties tend to be small compared to the two-decade changes. Attention must then turn to the issue of systematic errors in the model and state estimate. These will never be zero, but because of the data-fitting in the state estimation process, they are expected to be much-reduced compared to those found in unadjusted climate models.

A full discussion of the global structures and causes of the various fields appearing in the means and in the heating/cooling, salinification/freshening, elevation increases/decreases in time and space requires a specialized study of each field separately and is not attempted here.

References

Boyer, T., C. M. Domingues, S. A. Good, G. C. Johnson, J. M. Lyman, M. Ishii, V. Gouretski, J. K. Willis, J. Antonov, S. Wijffels, J. A. Church, R. Cowley and N. L. Bindoff (2016). Sensitivity of Global Upper-Ocean Heat Content Estimates to Mapping Methods, XBT Bias Corrections, and Baseline Climatologies.Journal of Climate 29(13): 4817-4842.

Boyer, T. P., S. Levitus, J. I. Antonov, R. A. Locarnini and H. E. Garcia (2005). Linear trends in salinity for the World Ocean, 1955-1998.Geophysical Research Letters 32(1).

Brogan, W. (1991). Modern Control Theory. Third Ed., Prentice-Hall, Englewood Cliffs, NJ.

Church, J. A., P. U. Clark, A. Cazenave, J. M. Gregory, S. Jevrejeva, A. Levermann, M. A. Merrifield, G. A. Milne, R. S. Nerem, P. D. Nunn, A. J. Payne, W. T. Pfeffer, D. Stammer and A. S. Unnikrishnan (2013). Sea-Level Rise by 2100.Science 342(6165): 1445-1445.

Consortium, E. (2017a). A Twenty-Year Dynamical Oceanic Climatology: 1994-2013. Part 1: Active Scalar Fields: Temperature, Salinity, Dynamic Topography, Mixed-Layer Depth, Bottom Pressure.Online at MIT DSpace.

Consortium, E. (2017b). A Twenty-Year Dynamical Oceanic Climatology: 1994-2013. Part 2: Velocities and Property Transports. MIT DSpace.

Efron, B. and R. Tibshirani (1993). An Introduction to the Bootstrap. New York, Chapman & Hall.

Evensen, G. (2009). Data Assimilation: The Ensemble Kalman Filter, Springer Verlag.

Forget, G., J.-M. Campin, P. Heimbach, C. Hill, R. Ponte and C. Wunsch (2015). ECCO version 4: an integrated framework for non-linear inverse modeling and global ocean state estimation.Geosci. Model Dev. 8: 3071-3104.

Forget, G. and R. M. Ponte (2015). The partition of regional sea level variability.Progress in Oceanography 137: 173-195.

Fukumori, I., P. Heimbach, R. M. Ponte and C. Wunsch (2017). A dynamically-consistent ocean climatology and its temporal variations.Bull. Am. Met. Soc. Submitted.

Fukumori, I. and C. Wunsch (1991). Efficient representation of the North Atlantic hydrographic and chemical distributions.Prog. in Oceanog., 27: 111-195.

Gardiner, C. W. (2004). Handbook of Stochastic Methods for Physics, Chemistry, and the Natural Sciences, 3rd Ed., Springer-Verlag, Berlin.

Goodwin, G. C. and K. S. Sin (1984). Adaptive Filtering Prediction and Control, Prentice-Hall, Englewood Cliffs, N. J.

Intergovernmental Oceanographic Commission, I. (2010). The International Thermodynamic Equation of Seawater 2010: Calculation and Use of Thermodynamic Properties, UNESCO,

Paris.

Kalmikov, A. and P. Heimbach (2014). A Hessian-based method for uncertainty quantification in global ocean state estimation. Siam Journal on Scientific Computing 36(5): S267-S295.

Levitus, S., J. I. Antonov, T. P. Boyer, H. E. Garcia and R. A. Locarnini (2005). Linear trends of zonally averaged thermosteric, halosteric, and total steric sea level for individual ocean basins and the world ocean, (1955-1959)-(1994-1998).Geophysical Research Letters 32(16).

Liang, X., C. Wunsch and M. Spall (2017). Global ocean vertical velocity from a dynamically consistent ocean state estimate. J. Geophys. Res. in press.

Lyman, J. M. and G. C. Johnson (2014). Estimating Global Ocean Heat Content Changes in the Upper 1800 m since 1950 and the Influence of Climatology Choice*.Journal of Climate 27(5): 1945-1957.

Majda, A. J. and J. Harlim (2012). Filtering Complex Turbulent Systems. Cambridge, Cambridge University Press.

Mudelsee, M. (2014). Climate Time Series Analysis: Classical Statistical and Bootstrap Methods, Springer.

Munk, W. (2003). Ocean Freshening, Sea Level Rising.Science 300(5628): 2041-2043.

Nerem, R. S., E. Leuliette and A. Cazenave (2006). Present-day sea-level change: A review.Comptes Rendus Geoscience 338(14-15): 1077-1083.

Nerem, R. S., E. Leuliette and A. Cazenave (2006). Present-day sea-level change: A review.Comptes Rendus Geoscience 338(14-15): 1077-1083.

Ocaña, V., E. Zorita and P. Heimbach (2016). Stochastic trends in sea level rise.J. Geophys. Res. 121: doi:10.1002/2015JC011301.

Peltier, W. R. (2009). Closure of the budget of global sea level rise over the GRACE era: the importance and magnitudes of the required corrections for global glacial isostatic adjustment.Quaternary Science Reviews 28(17-18): 1658-1674.

Purkey, S. G. and G. C. Johnson (2010). Warming of Global Abyssal and Deep Southern Ocean Waters between the 1990s and 2000s: Contributions to Global Heat and Sea Level Rise Budgets.Journal of Climate 23(23): 6336-6351.

Strogatz, S. H. (2015). Nonlinear dynamics and chaos : with applications to physics, biology, chemistry, and engineering. Boulder, CO, Westview Press.

Wadhams, P. and W. Munk (2004). Ocean freshening, sea level rising, sea ice melting.Geophysical Research Letters 31(11).

Worthington, L. V. (1981). The water masses of the world ocean: some results of a fine-scale census. in, Evolution of Physical Oceanography. Scientific Surveys in Honor of Henry Stommel. B. A. Warren and C. Wunsch, The MIT Press, Cambridge (available online at

http://ocw.mit.edu/ans7870/textbooks/Wunsch/wunschtext.htm): 42-69.

Wunsch, C. (2002). Oceanic age and transient tracers: Analytical and numerical solutions.Journal of Geophysical Research-Oceans 107(C6).

Wunsch, C. (2006). Discrete Inverse and State Estimation Problems: With Geophysical Fluid Applications. Cambridge ; New York, Cambridge University Press.

Wunsch, C. (2016). Global ocean integrals and means, with trend implications. Annual Review of Marine Science, Vol 8. C. A. Carlson and S. J. Giovannoni. 8: 1-33.

Wunsch, C. and P. Heimbach (2013). Dynamically and kinematically consistent global ocean circulation state estimates with land and sea ice. in Ocean Circulation and Climate, 2nd Edition. J. C. G. Siedler, W. J. Gould, S. M. Griffies, Eds., Elsevier: 553-579.

Wunsch, C. and P. Heimbach (2014). Bidecadal thermal changes in the abyssal ocean and the observational challenge.J. Phys. Oc. 44: 2013-2030.

Figure Captions

1. (a) Histogram values over the full volume of the 20-year average potential temperature in ECCO v4 (nov 2016). (b) Values in (a) weighted as $\overline{T}_i a_i$ where $\overline{T}_i$ is the time mean temperature in model volume cell i, and a_i is the fraction of the total volume of fluid represented. (c) Residual of $a_i \overline{T}_i$ after removal of first two pairs of singular vectors. Skewness of the original values is greatly reduced.

2. Twenty-year mean temperature at 105m ($°$C). Inset shows the multi-modal histogram of values. The gyre structure is dominant and regarded here as a deterministic element of the field. (From Fukumori et al., 2017)

3. (a) The means computed from 50 bootstrap samples of N each of the 20-year mean volume-weighted temperatures. The mean of means is 3.54 degrees with a standard deviation of $3.1 \times 10^{-3°}$. Singular values, λ_j (c) Bootstrap means with the first 3 singular vector pairs removed. Standard error is reduced to $6.8 \times 10^{-4°}$C (d) Cumulative sum of normalized λ_i^2, $S(J)$ showing that removal of the first three singular value pairs reduces the variance by about 96%.

4. Variance with depth of the 20-year mean temperature before and after of removal of 3 singular vector pairs. After removal, the variance is closer to uniform with depth.

5. (a-c) first three of the $\mathbf{u}_i$ singular vectors of time-mean temperature. (d) Corresponding $\mathbf{v}_i$ (d-f) are the histograms of values in the corresponding $\mathbf{u}_i$. Those for $\mathbf{u}_1$ are distinctly non-normal and almost all negative corresponding to the negative values in $\mathbf{u}_1$. Here $\mathbf{u}_i, \mathbf{v}_i$ are regarded as dimensionless with physical dimensions carried by the singular values λ_i.

6. Residual at 555m of volume weighted temperatures after removal of the first three singular vector pairs. This residual field and those at other depths are treated as stochastic.

7. Raw values (a) of model 20-year average salt. (b) shows the values weighted by relative volumes, $a_i \overline{S}_i$ and (c) is the same as (b) after removal of first 2 singular vectors.

8. Same as Fig. 3 except for salinity.

9. (a-c) $100\mathbf{u}_i$ $i = 1, 2, 3$ for the 20-year mean salinity. Distribution of values is highly non-normal. (d) Corresponding $\mathbf{v}_i$ in depth.

10. Salinity residual at 555m after removal of the first three singular vector pairs (g/kg volume weighted).

11. Twenty-year mean η relative to the geoid (m). The large-scale gyre structure is deterministic, but the extent to which the remaining structures are stochastic remains unclear. (From Fukumori et al., 2017) Arrows indicate the sense of the corresponding geostrophic flow.

12. Residual of the 20-year mean of η after removal of the 3 lowest singular vector pairs.

13. (Upper panel) Difference of temperatures in 2013 and 1994 at 105 m. The spatial complexity is apparent. High outliers in the Pacific warm pool have been truncated in the plot. Physically interpretable changes by region, particularly in the tropics, suggest an at least partially determinstic structure. Lower panel is similar, except at 3900 m and showing the distinct difference between high southern latitudes and the rest of the world ocean. (cf. Wunsch and Heimbach, 2014).

14. Variance (solid line) of the temperature difference as a function of depth. Dashed line is the same result after removal of the first 2 pairs of singular vectors, producing a much more uniform result.

15. First three $\mathbf{u}_i$ and first 5 $\mathbf{v}_i$ of the temperature difference fields for 1994 and 2013.

16. Histogram of values of the difference in temperature over 20 years (upper left panel). Volume weighted difference (upper right panel) of values in the left panel. Lower panels show the bootstrapped temperature difference statistics without removing the two lowest singular vector structures (c) and after they are removed (e). (d), (f) are the singular values and their cumulative square normalized to one.

17. Salinity differences 2013 minus 1994 at 105m depth, g/kg. This field might be treated as wholly stochastic, but the first two singular value pairs are removed prior to bootstrapping the mean.

18. Histogram of salinity differences over 20 years (upper left panel) and as weighted by relative volumes, $\sigma_i = a_i S_i$ (upper right panel). Weighted distribution values are more nearly Gaussian than salinity itself. Lower panels. Same as Fig. 3 except for the salinity differences between 2013 and 1994. No singular value dominates and there is no obvious deterministic component in the current definition. The ocean circulation itself is capable of considerable randomization.

19. Difference (m) of the mean elevation in 2013 and 1994. Note the long positive tail in the histogram.

20. Vertically integrated mean temperatures over 20 years. Upper panel shows the result for 100m, 700m and top-to-bottom. Lower panel shows the values to 3600m, the abyssal component (below 3600m) and a repetition of the total value. Heat content change requires accounting for the different masses of these layers. The top 100m is much noisier than the thicker volumes below.

21. Bootstrapped slope from annual means of the top-to-bottom temperature anomaly with the lowest pair of singular values removed. Bootstrapped mean is $3.1 \times 10^{-5 \circ}$C/y with a standard error of $5 \times 10^{-4 \circ}$C/y.

22. Time-dependent $\mathbf{v}_i, i = 1, 2, 3$ for temperature slope estimates. $\mathbf{v}_1$, with a gross overall

trend, is deemed deterministic, while higher $\mathbf{v}_i$ and corresponding spatial $\mathbf{u}_i$ are treated as stochastic.

23. Integrated salt anomaly for each year to various depths. Curve for the total is repeated in both panels and shows an overall freshening, top-to-bottom. As in temperature, the upper layer is quite noisy.

24. (a) First singular vector $\mathbf{u}_1$ of the annual mean salt anomalies, but which is *not* here suppressed in the uncertainty calculation. (b) First 3 $\mathbf{v}_i$ of the annual mean salinity anomalies. $\mathbf{v}_1$ corresponds to an overall trend, but whose sign depends upon the sign in (a), and is removed for the uncertainty calculation. The positive slope in $\mathbf{v}_1$ corresponds to a freshening in regions where $\mathbf{u}_1$ is negative in (a).

25. Annual means of the anomaly of η (upper panel, m) and of the differences of successive years (lower panel, m/y).

26. (a) $\mathbf{u}_1$ singular vector for annual anomalies of η. The spatial pattern has a strong ENSO-like component, but the temporal coefficient (b) includes a trend-like component superimposed. (b) Temporal $\mathbf{v}_i$ for the annual mean anomalies of η. $\mathbf{v}_1$ has a trend-like behavior while $\mathbf{v}_{2,3}$ are influenced by the ENSO event of 1997-1998. These are treated here as stochastic.
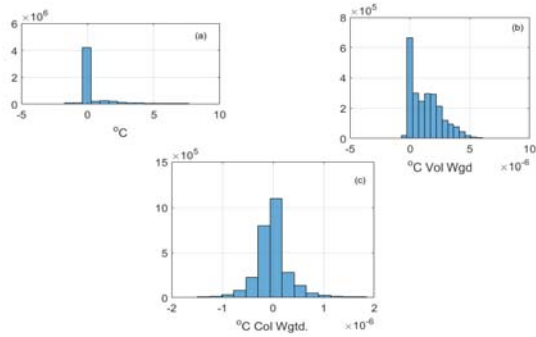
Figure 1: (a) Histogram values over the full volume of the 20-year average potential temperature in ECCO v4 (nov 2016). (b) Values in (a) weighted as $\overline{T_i}a_i$ where $\overline{T_i}$ is the time mean temperature in model volume cell i, and a_i is the fraction of the total volume of fluid represented. (c) Residual of $a_i\overline{T_i}$ after removal of first two pairs of singular vectors. Skewness of the original values is greatly reduced.
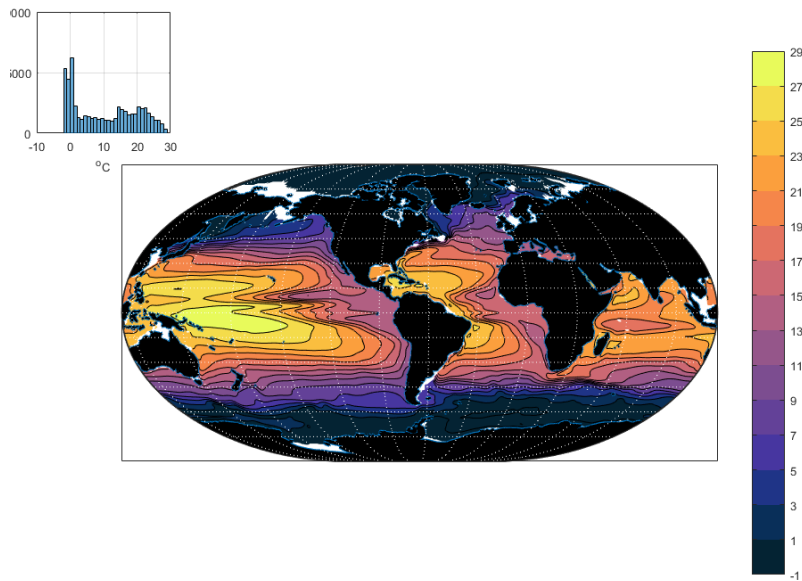
Figure 2: Twenty-year mean temperature at 105m (°C). Inset shows the multi-modal histogram of values. The gyre structure is dominant and regarded here as a deterministic element of the field. (From Fukumori et al., 2017)

4
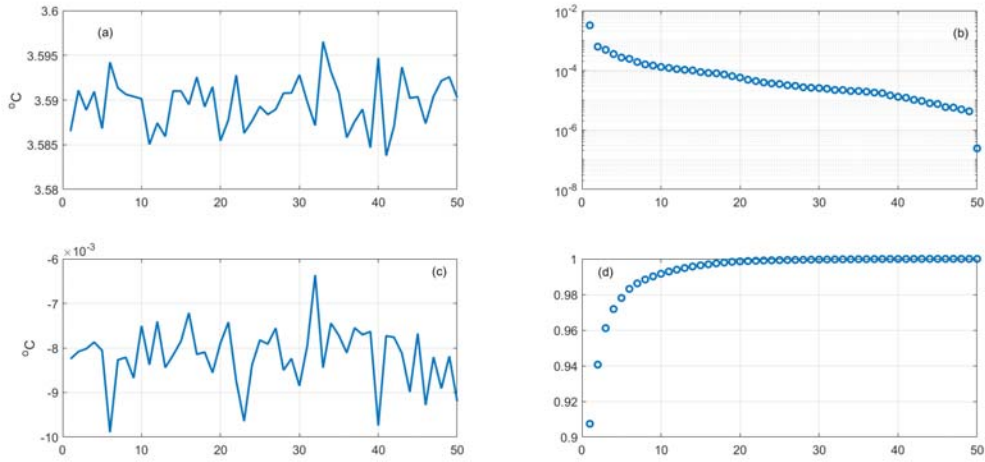
Figure 3: (a) The means computed from 50 bootstrap samples of N each of the 20-year mean volume-weighted temperatures. The mean of means is 3.54 degrees with a standard deviation of $3.1 \times 10^{-3\circ}$. Singular values, λ_j (c) Bootstrap means with the first 3 singular vector pairs removed. Standard error is reduced to $6.8 \times 10^{-4\circ}$C (d) Cumulative sum of normalized λ_i^2, $S(J)$ showing that removal of the first three singular value pairs reduces the variance by about 96%.
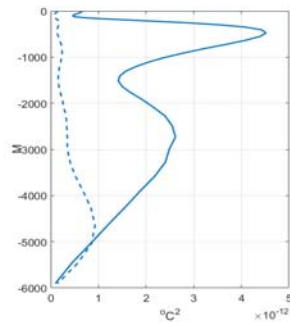
Figure 4: Variance with depth of the 20-year mean temperature before and after of removal of 3 singular vector pairs. After removal, the variance is closer to uniform with depth.
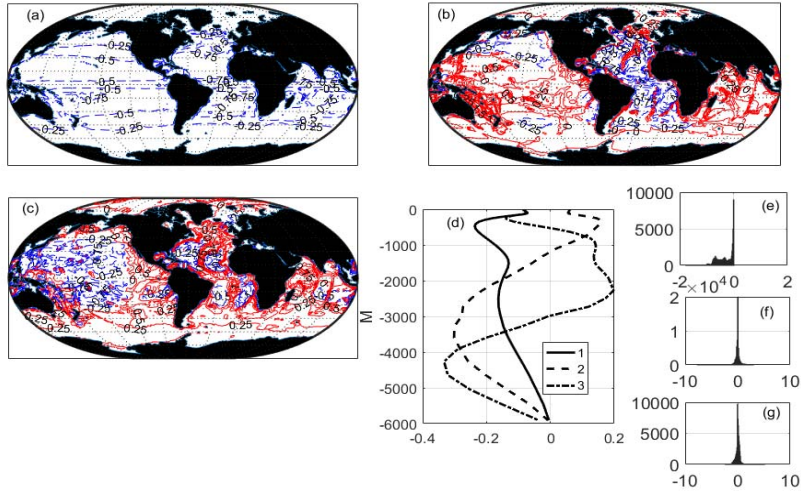
Figure 5: (a-c) first three of the $\mathbf{u}_i$ singular vectors of time-mean temperature. (d) Corresponding $\mathbf{v}_i$.
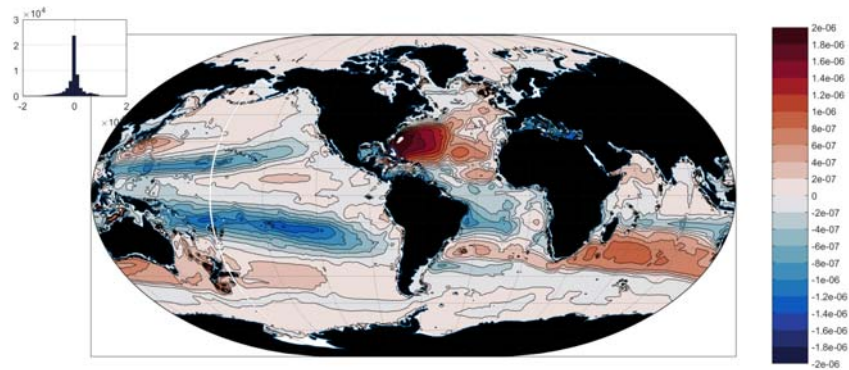
Figure 6: Residual at 555m of volume weighted temperatures after removal of the first three singular vector pairs. This residual field and those at other depths are treated as stochastic.
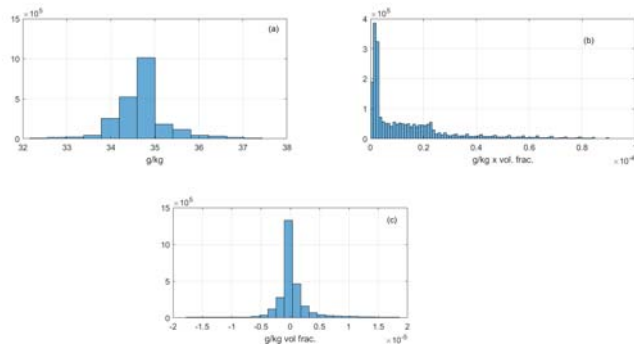
Figure 7: Raw values (a) of model 20-year average salt. (b) shows the values weighted by relative volumes, $a_i \bar{S}_i$ and (c) is the same as (b) after removal of first 2 singular vectors.
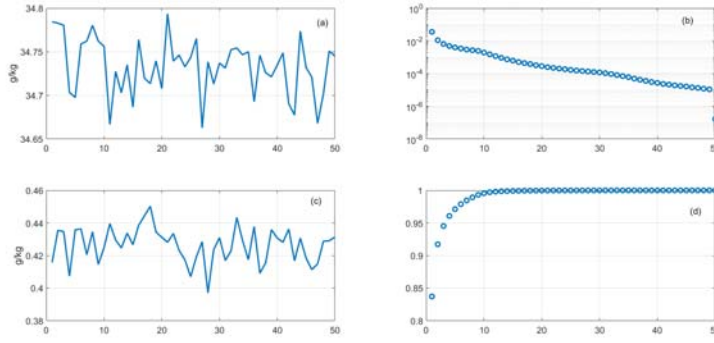
Figure 8: Same as Fig. 3 except for salinity.
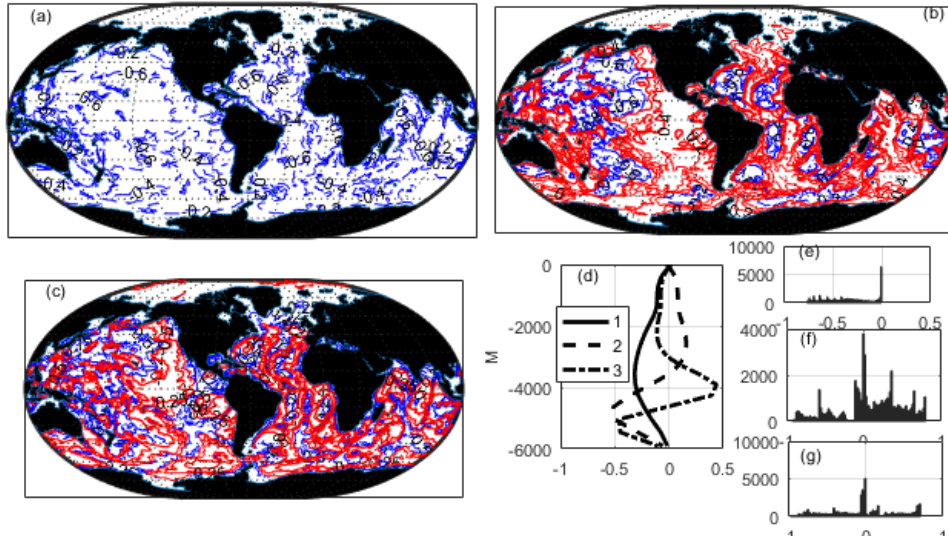
Figure 9: (a-c) $100\mathbf{u}_i$ $i = 1, 2, 3$ for the 20-year mean salinity. Distribution of values is highly non-normal. Red contours are positive, blue are negative. (d) Corresponding $\mathbf{v}_i$ in depth.
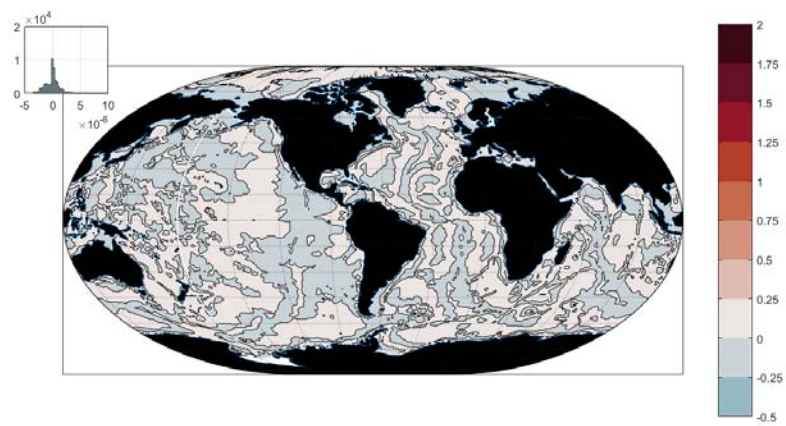
Figure 10: Salinity residual at 555m after removal of the first three singular vector pairs (g/kg volume weighted).
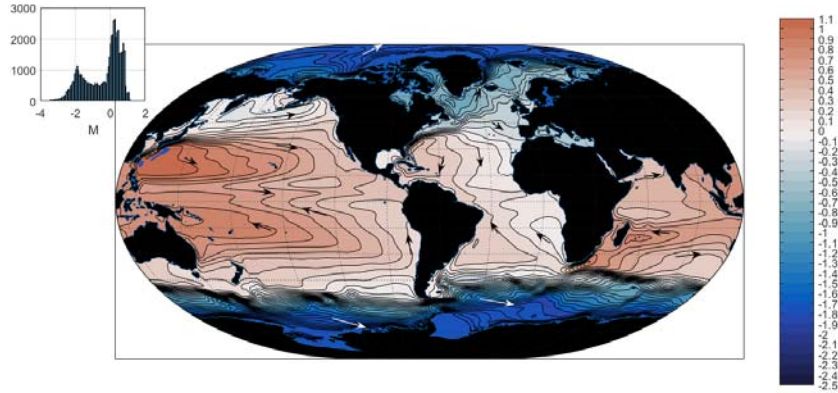
Figure 11: Twenty-year mean η relative to the geoid (m). The large-scale gyre structure is deterministic, but the extent to which the remaining structures are stochastic remains unclear. (From Fukumori et al., 2017) Arrows indicate the sense of the corresponding geostrophic flow.
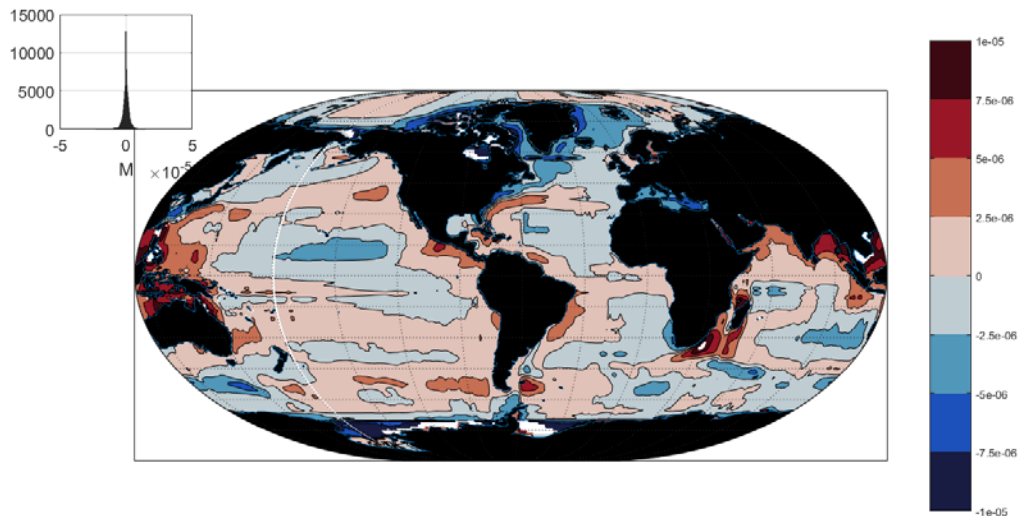
Figure 12: Residual of the 20-year mean of η after removal of the 3 lowest singular vector pairs.
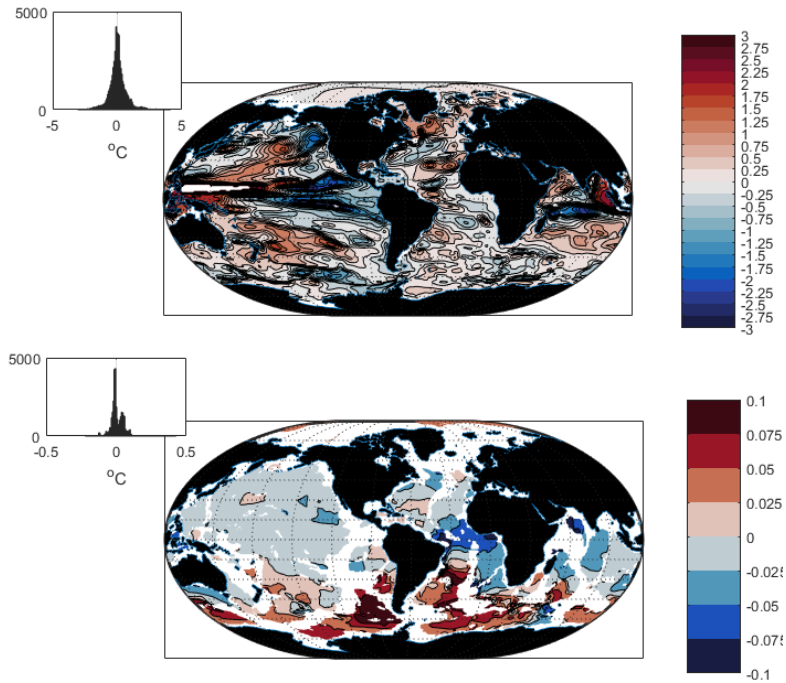
Figure 13: (Upper panel) Difference of temperatures in 2013 and 1994 at 105 m. The spatial complexity is apparent. High outliers in the Pacific warm pool have been truncated in the plot. Physically interpretable changes by region, particularly in the tropics, suggest an at least partially determinstic structure. Lower panel is similar, except at 3900 m and showing the distinct difference between high southern latitudes and the rest of the world ocean. (cf. Wunsch and Heimbach, 2014).
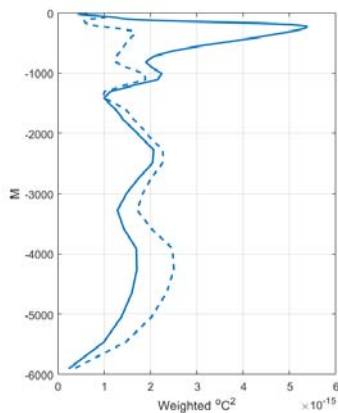
Figure 14: Variance (solid line) of the temperature difference as a function of depth. Dashed line is the same result after removal of the first 2 pairs of singular vectors, producing a much more uniform result.
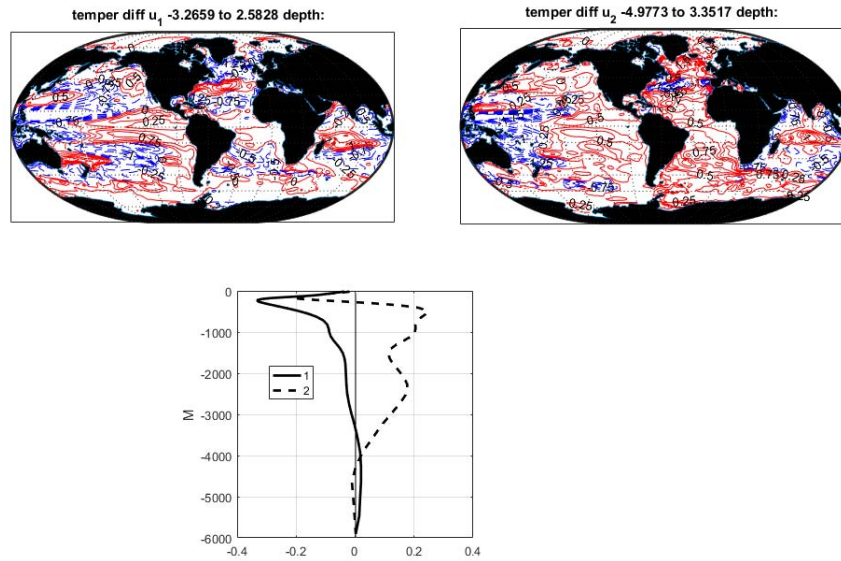
Figure 15: First two $\mathbf{u}_i$ and first 2 $\mathbf{v}_i$ of the temperature difference fields for 1994 and 2013.
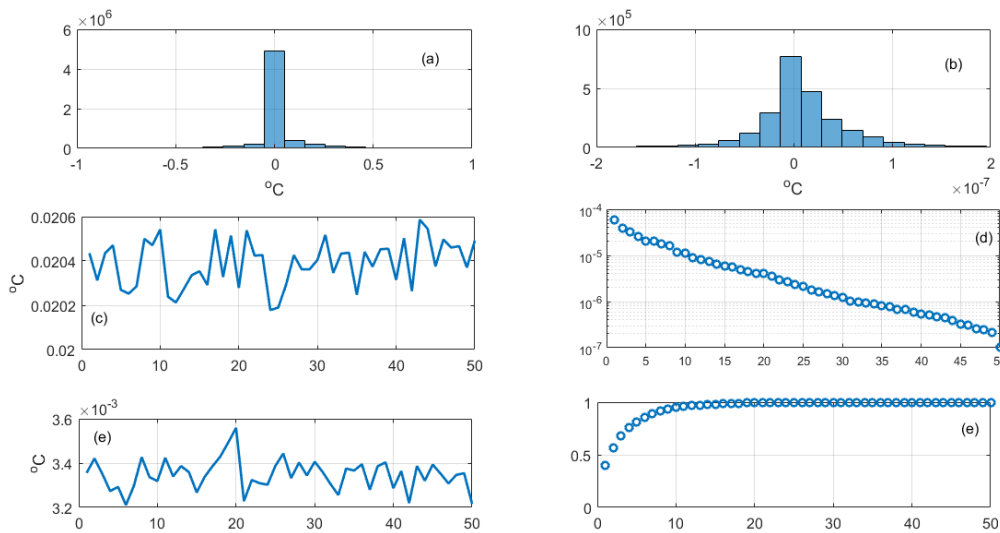
Figure 16: Histogram of values of the difference in temperature over 20 years (upper left panel). Volume weighted difference (upper right panel) of values in the left panel. Lower panels show the bootstrapped temperature difference statistics without removing the two lowest singular vector structures (c) and after they are removed (e). (d), (f) are the singular values and their cumulative square normalized to one.
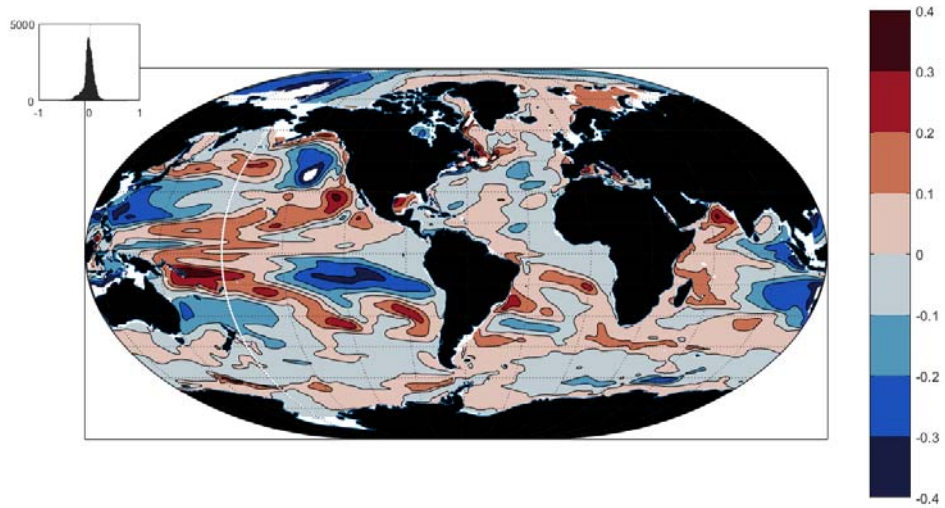
Figure 17: Salinity differences 2013 minus 1994 at 105m depth, g/kg. This field might be treated as wholly stochastic, but the first two singular value pairs are removed prior to bootstrapping the mean.
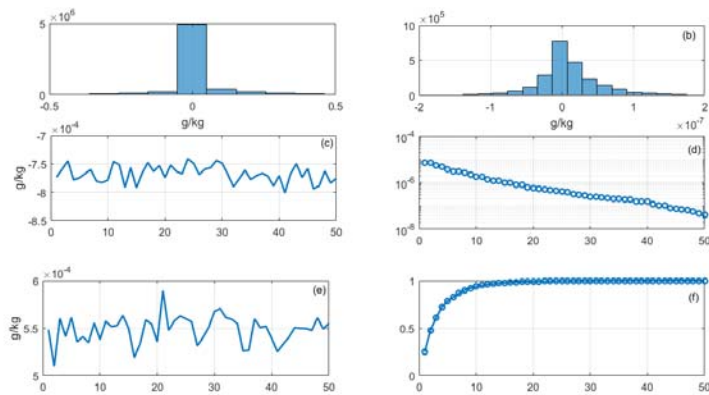
Figure 18: Histogram of salinity differences over 20 years (upper left panel) and as weighted by relative volumes, $\sigma_i = a_i S_i$ (upper right panel). Weighted distribution values are more nearly Gaussian than salinity itself. Lower panels. Same as Fig. 3 except for the salinity differences between 2013 and 1994. No singular value dominates and there is no obvious deterministic component in the current definition. The ocean circulation itself is capable of considerable randomization.
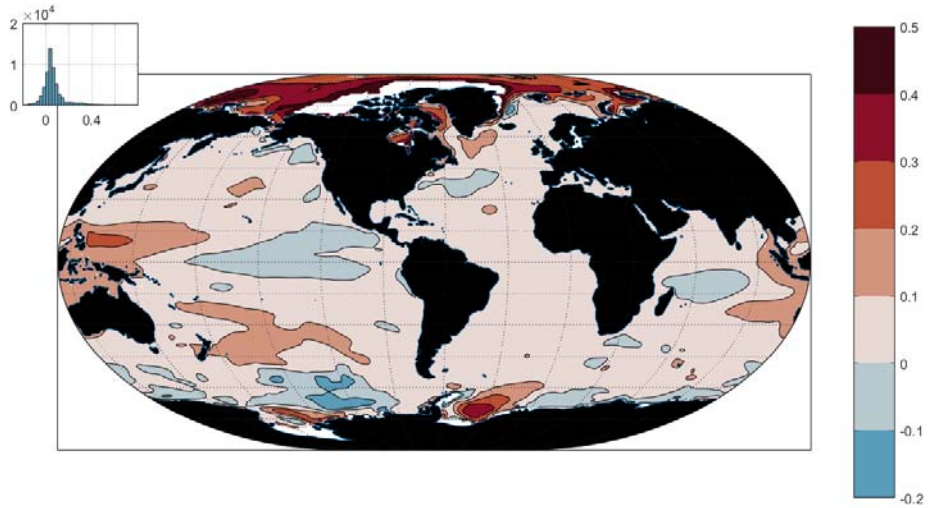
Figure 19: Difference (m) of the mean elevation in 2013 and 1994. Note the long positive tail in the histogram.
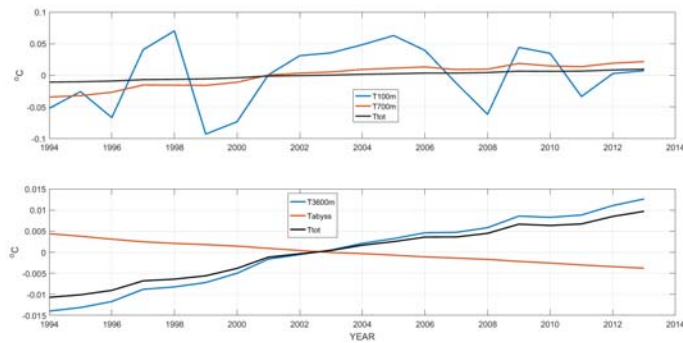
Figure 20: Vertically integrated mean temperatures over 20 years. Upper panel shows the result for 100m, 700m and top-to-bottom. Lower panel shows the values to 3600m, the abyssal component (below 3600m) and a repetition of the total value. Heat content change requires accounting for the different masses of these layers. The top 100m is much noisier than the thicker volumes below.
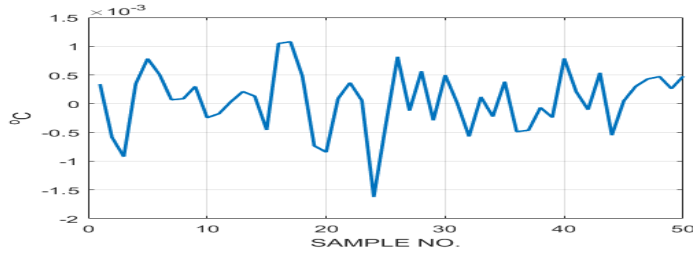
Figure 21: Bootstrapped slope from annual means of the top-to-bottom temperature anomaly with the lowest pair of singular values removed. Bootstrapped mean is $3.1 \times 10^{-5 \circ}$C/y with a standard error of $5 \times 10^{-4 \circ}$C/y.
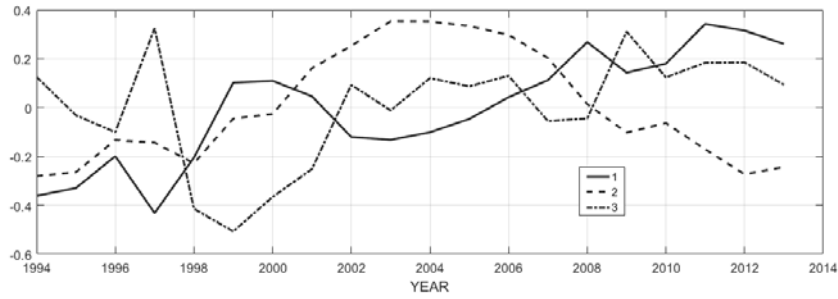

Figure 22: Time-dependent $\mathbf{v}_i$, $i = 1, 2, 3$ for temperature slope estimates. $\mathbf{v}_1$, with a gross overall trend, is deemed deterministic, while higher $\mathbf{v}_i$ and corresponding spatial $\mathbf{u}_i$ are treated as stochastic.
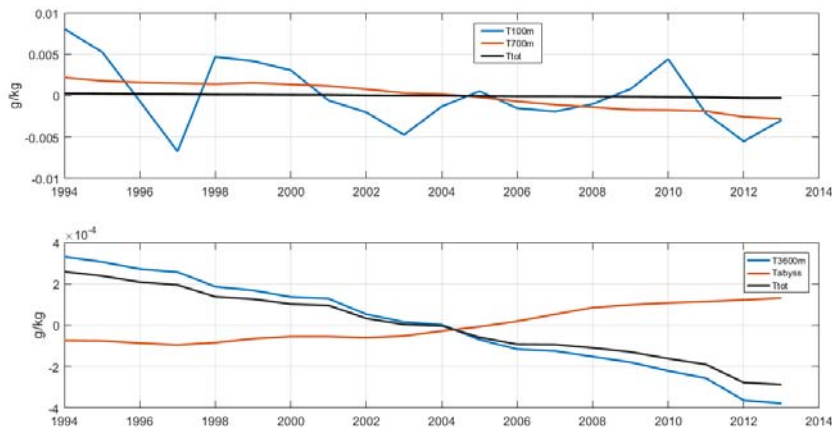

Figure 23: Integrated salt anomaly for each year to various depths. Curve for the total is repeated in both panels and shows an overall freshening, top-to-bottom. As in temperature, the upper layer is quite noisy.
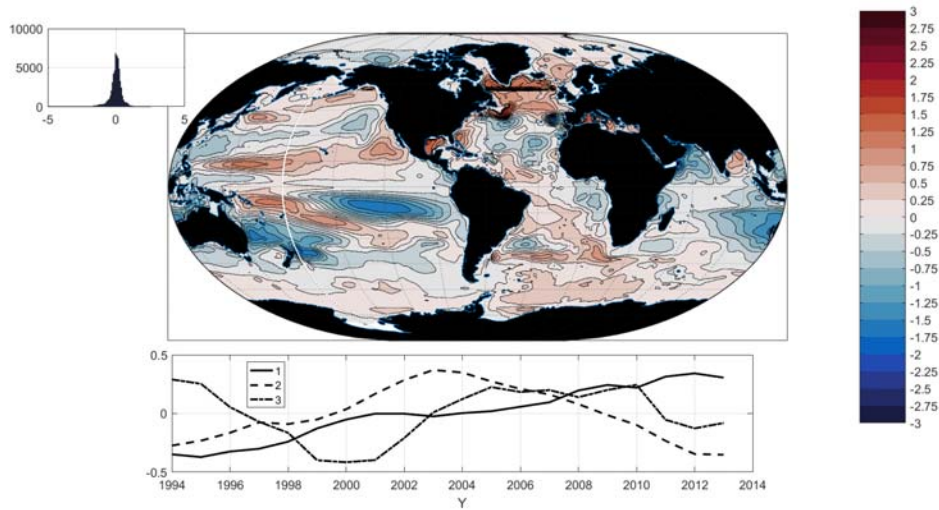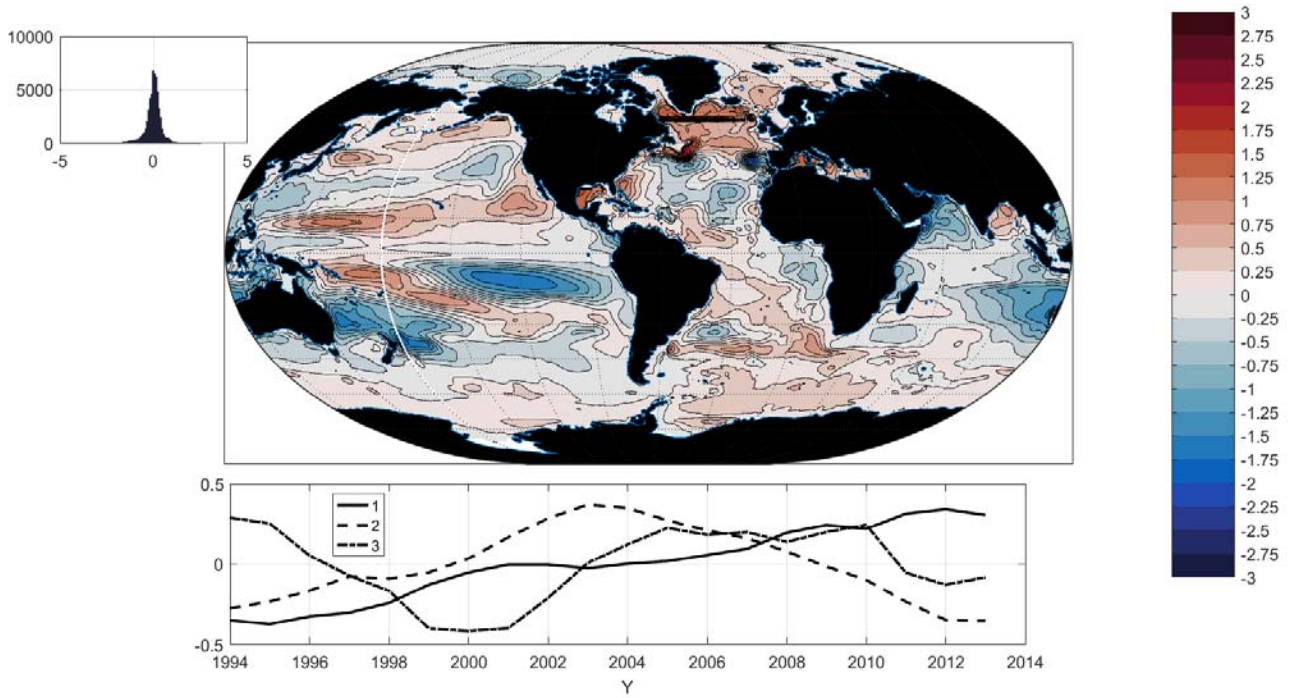
14

Figure 24: (a) First singular vector $\mathbf{u}_1$ of the annual mean salt anomalies, but which is *not* here suppressed in the uncertainty calculation. (b) First 3 $\mathbf{v}_i$ of the annual mean salinity anomalies. $\mathbf{v}_1$ corresponds to an overall trend, but whose sign depends upon the sign in (a), and is removed for the uncertainty calculation. The positive slope in $\mathbf{v}_1$ corresponds to a freshening in regions where $\mathbf{u}_1$ is negative in (a).
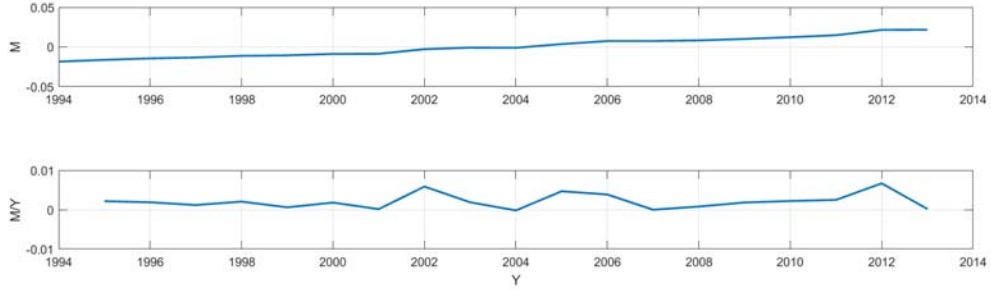
Figure 25: Annual means of the anomaly of η (upper panel, m) and of the differences of successive years (lower panel, m/y).
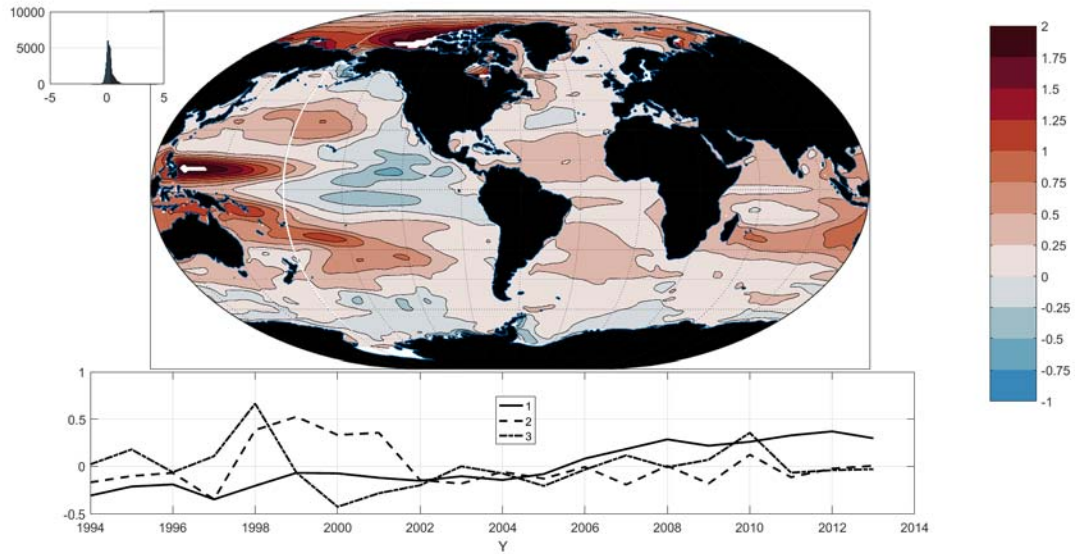

Figure 26: (a) $\mathbf{u}_1$ singular vector for annual anomalies of η. The spatial pattern has a strong ENSO-like component, but the temporal coefficient (b) includes a trend-like component superimposed. (b) Temporal $\mathbf{v}_i$ for the annual mean anomalies of η. $\mathbf{v}_1$ has a trend-like behavior while $\mathbf{v}_{2,3}$ are influenced by the ENSO event of 1997-1998. These are treated here as stochastic.

16